

## Article

# Optical Design of a Miniaturised Solar Magnetograph for Space Applications

Ariadna Calcines Rosario <sup>1,\*</sup>, Lucie M. Green <sup>2</sup>, Alan Smith <sup>2</sup> and David M. Long <sup>3</sup><sup>1</sup> Centre for Advanced Instrumentation, Department of Physics, Durham University, Durham DH1 3LE, UK<sup>2</sup> Mullard Space Science Laboratory, University College London, Holmbury St. Mary, Dorking, Surrey RH5 6NT, UK<sup>3</sup> Astrophysics Research Centre, School of Mathematics and Physics, Queen's University Belfast, University Road, Belfast BT7 1NN, UK

\* Correspondence: ariadna.calcines@durham.ac.uk

**Abstract:** Measuring the Sun's magnetic field is a key component of monitoring solar activity and forecasting space weather. The main goal of the research presented in this paper is to investigate the possibility of reducing the dimensions and weight of a solar magnetograph while preserving its optical quality. This article presents a range of different designs, along with their advantages and disadvantages, and an analysis of the optical performance of each. All proposed designs are based on the magneto-optical filter (MOF) technique. As a result of the design study, a miniaturised solar magnetograph is proposed with an ultra-compact layout. The dimensions are 345 mm × 54 mm × 54 mm, and the optical quality is almost at the diffraction limit. The design has an entrance focal ratio of F/17.65, with a plate scale of 83.58 arcsec/mm at the telescope image focal plane, and produces a magnification of 0.79. The field of view is 1920 arcsec in diameter, equivalent to ±0.27 degrees, sufficient to cover the entire solar disk.

**Keywords:** solar magnetograph; space weather; space sciences; solar instrumentation; miniaturised optics



**Citation:** Calcines Rosario, A.; Green, L.M.; Smith, A.; Long, D.M. Optical Design of a Miniaturised Solar Magnetograph for Space Applications. *Aerospace* **2023**, *10*, 1028. <https://doi.org/10.3390/aerospace10121028>

Academic Editor: Stanislav Gordeyev

Received: 6 October 2023

Revised: 30 November 2023

Accepted: 2 December 2023

Published: 13 December 2023



**Copyright:** © 2023 by the authors. Licensee MDPI, Basel, Switzerland. This article is an open access article distributed under the terms and conditions of the Creative Commons Attribution (CC BY) license (<https://creativecommons.org/licenses/by/4.0/>).

## 1. Introduction

The Sun is a centrally important star. Its relatively close proximity means that it can be spatially resolved, providing information that is vital for understanding not only our Sun but stars in general [1]. The Sun is an active star, in that it emits a wind of magnetised plasma that flows over and effects all Solar System objects and it sporadically ejects vast clouds of magnetised plasma (known as coronal mass ejections), bursts of electromagnetic radiation (known as solar flares), and high-energy particles that affect Solar System bodies. The variations that these forms of activity create in the near-Earth space environment are collectively known as space weather [2]. Space weather can have deleterious impacts on modern life through disruptions to electricity transmission, high-frequency radio communication, and navigation systems.

To understand the physics of the Sun, and the origins of solar activity and space weather, it is crucial to measure and monitor the solar magnetic field. So-called non-potential magnetic fields harbour energy that powers the various forms of solar activity [3], and certain magnetic field configurations form in the Sun's atmosphere prior to the occurrence of flares and coronal mass ejections [4]. In addition, measurements of the magnetic field in the photosphere are used as the boundary condition for space weather tools used to model the solar wind conditions and the propagation of CMEs to the Earth, such as WSA-ENLIL [5] or EUHFORIA [6].

To this end, space and ground-based instrumentation monitoring the Sun has, for decades, included magnetographs that measure the polarisation state of the light of the Sun to determine the magnetic field strength and direction. Most of these instruments exploit the Zeeman effect in which a magnetic field induces both energy-level splitting and polarization

of the emitted light. Magnetographs that use this technique make measurements centred on a magnetically sensitive spectral line produced in the lower solar atmosphere. However, the capability to determine the magnetic field in the solar corona via the Hanle effect is growing (e.g., the Daniel K. Inouye Solar Telescope Visible Spectro-Polarimeter [7]).

Current designs for ground and space-based solar magnetographs utilising the Zeeman effect make use of both filtergraph (e.g., the Helioseismic and Magnetic Imager Telescope on the Solar Dynamics Observatory [8]) and spectrograph techniques (the Solar Optical Telescope onboard Hinode [9]) to provide information on the magnetic field. The former allows for relatively high-cadence full-disc magnetograms to be made but with fewer measurements taken across the selected spectral line. The latter provides partial field of view magnetograms that take longer to construct but which have significantly increased spectral resolution and therefore provide higher precision. Space-based magnetographs have an additional design constraint in that they must operate within limited mass, size, and power budgets. The Michelson Doppler Imager instrument onboard the SOHO spacecraft has a total mass of 56 kg [10], the HMI instrument onboard the Solar Dynamics Observatory has a mass of 73 kg, and the Polarimetric and Helioseismic Imager instrument onboard Solar Orbiter has a mass of 35 kg [11]. With a view to the future, smaller and more lightweight magnetographs can be more readily employed and offer the practicality of inclusion on a wider range of missions. A truly compact and lightweight magnetograph opens up the possibility of multiple flight opportunities, including in a constellation that could provide near full-Sun coverage.

One solution to creating a small and lightweight magnetograph is to adapt a technique that has been used in ground-based telescopes. That is, to utilise magneto-optical filters (MOFs; [12]). MOFs contain an elemental vapour immersed in a strong magnetic field, and so only photons close to the atomic resonance frequency pass through, thereby creating a narrow band filter. For example, a potassium vapour filters all photons except those originating in the mid-photosphere, whilst a sodium vapour filters all except those originating in the lower chromosphere. MOFs have a high throughput and wavelength stability and reject the continuum light of the Sun, only allowing through light from the red and blue wings of the Zeeman broadened/split selected spectral line, allowing only these photons to be analysed. Ground-based telescopes having successfully implemented the MOF technology include, for example, MOTH at the Mees Solar Observatory in Hawaii, MOTH II, located at the South Pole in Antarctica [13], and the Tor Vergata Synoptic Solar Telescope (TSST) in La Palma, Spain [14,15]. Previous studies have demonstrated that the use of a magneto-optical filter could lead to a space-based magnetograph design of reduced size and mass (e.g., [16–18]). The study of [18] conceived a space-based magnetograph of mass 14 kg with dimensions  $850 \times 150 \times 150$  mm. In this paper, we build on the previous work to make steps towards a conceptual design of a compact ( $800 \text{ mm} \times 200 \text{ mm} \times 200 \text{ mm}$ ) lightweight (<15 kg) magnetograph. We search for an optimum optical configuration in order to compress the size of the instrument whilst preserving instrument performance.

## 2. Magneto-Optical Filter Technique

A magneto-optical filter (MOF) is a narrow band filter that uses heated cells containing a vapour, such as sodium, immersed in a static magnetic field of about 2 kGauss. The vapour cells are typically a few centimetres in each dimension. For potassium, the temperature should be greater than 373.15 K, typically 393.15 K. The temperature of a cell is kept to  $\pm 1$  K and the cells are placed in vacuum chambers to prevent convection around them. Overall, two vapour cells are needed (labelled as “MOF” and the wing selector, WS, in Figure 1), along with a series of quarter and half-wave plates and two linear polarisers (P1 and P2), as shown in Figure 1. The axes of P1 and P2 are orthogonal to each other and so act as crossed polarisers. The wavelength of the MOF is not sensitive to the incidence angle of the light.

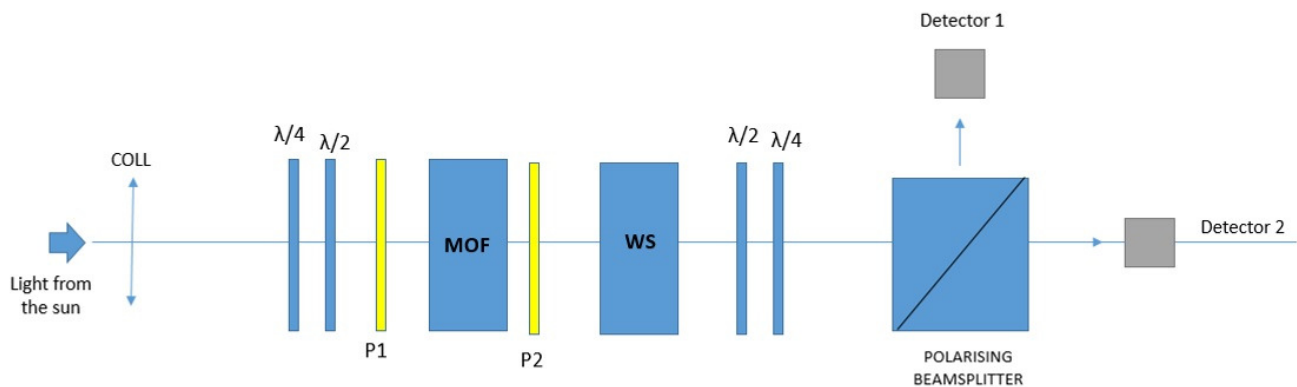


**Figure 1.** Schematic of a magnetograph layout that employs magneto-optical filters. The first magneto-optical filter in the optical path is labelled as the MOF and the second is labelled as the wing selector (WS). Also included are quarter-wave plates ( $\lambda/4$ ) and half-wave plates ( $\lambda/2$ ) to enable the passage of selected polarisation states. P1 and P2 are two linear polarisers whose axes are orthogonal to each other (crossed polarisers). Based on Barajas, Garcia, and Vo (2011).

Light from the Sun enters the optics and is collimated. A quarter-wave plate ( $\lambda/4$ ) at 45 degrees turns circularly polarised light into linearly polarised. After the quarter-wave plate, a half-wave plate ( $\lambda/2$ ) is used, whose orientation can be varied from 0 degrees to 45 degrees with respect to the axis of the linear polariser P1 (i.e., allows through linearly polarised light). The strong longitudinal magnetic field that is applied to the elemental vapour in the first MOF cell broadens/splits the spectral line and rotates the plane of polarisation of the light (via Faraday rotation). After the MOF cell, a second polariser, P2, is crossed with the input polariser so that ultimately only light of orthogonal linear polarisation passes through. This part of the magnetograph is sometimes called the “pre-filter” or the “filter selection MOF” (see, for example, [13]).

The wing selector converts the linearly polarised light into opposite circularly polarised light in the blue and red wings of the spectral line. Which wing is transmitted is controlled by the orientation of the quarter-wave plate so that full solar disk images can be made in the red and blue wings of the spectral line. A quarter-wave plate optically separates the circular polarisations into orthogonal linear polarisations. After the quarter-wave plate, the two orthogonal linear polarisations are separated using a polarising beam splitter, sending each one to a different detector in this configuration. It would be possible to have both on the same detector using a different polarising beam splitter.

The main factors found in existing solutions based on the MOF technique that pose limits on the spatial dimensions are:

- The optical components required for the instrument.
- The characteristics of the light required at each component location (i.e., collimated beam, polarisation state). This requires the use of optics, which enlarges the magnetograph layout.
- The cell dimensions, including its housing and electronics.
- The detectors, including electronics and cables.

Additional limitations come from the optimisation of the instrument performance. Two cells are required, with different magnetic fields. The magnetic field of the second cell (WS) shall be higher than that of the first cell. For both MOFs, the light needs to be linearly polarised—ideally collimated beams and with intermediate pupil images within each cell. For a better spectral response, collimated beams are also required for the half-wave plates, quarter-wave plates, and linear polarisers. To achieve this, some optical components are needed to generate the collimated beams and intermediate pupil images. All these components contribute to the total weight and also enlarge the dimensions of the instrument.

### 3. Layouts to Reduce Mass and Volume

Here, we explore four ideas that aim to reduce both the volume and the mass of a solar magnetograph, with a view on providing the basis of a design for a compact and lightweight space-based instrument after having evaluated a range of options.

#### 3.1. Option 1: Re-Imaging System before the Magneto-Optical Filter

A reduction in the size, and therefore mass, of the magneto-optical cells is possible if the diameter of the light beam is reduced. This can be achieved using a re-imaging system after the telescope image focal plane. This approach would also reduce the diameter of all optical components and lead to a reduction in the size of the mechanical mounts and an overall smaller mass and volume for the instrument. However, it would be necessary to evaluate the focal lengths required to achieve good optical performance for the re-imaging system. In order to minimise volume, the focal lengths would need to be as short as possible. A disadvantage of this approach would be a reduction of throughput associated with the addition of the optical surfaces for the re-imaging system. This would be  $\geq 0.96$ . A refractive solution (lenses) might be the most compact one if the focal lengths required are not too large since the angles in a reflective solution would increase the dimensions of the instrument in the direction perpendicular to that of the light propagation.

As shown in Figure 2, although the addition of the relay reduces the size of the beam and thus the size of all optical components, this advantage is negated since the focal lengths of the lenses required increase the total length of the magnetograph. For this reason, it was not considered in the final miniaturised magnetograph layout (see Section 4.3).

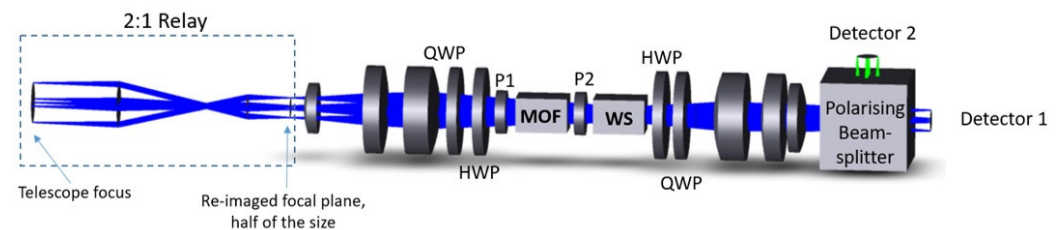


**Figure 2.** Optical design of a magnetograph using a 2:1 re-imaging system at the telescope focus. The total dimensions are 522.02 mm  $\times$  62.99 mm.

#### 3.2. Option 2: One Detector Instead of Two

In the layout of Figure 1, a polarising beam splitter separates the two orthogonal linear polarisations so that each one could be observed on a different detector. However, an alternative polarising beam splitter, such as a Wollaston prism, could be chosen to accommodate both polarisations within the same detector. Using one detector instead of two would reduce volume and mass.

A Wollaston prism separates light into two linearly polarised beams with orthogonal polarisation. The beams will be polarised according to the optical axis of the two right-angle prisms, which are cemented orthogonal prisms of birefringent material, such as calcite. At the exit, two beams are obtained, associated with the ordinary and extraordinary rays. These beams diverge due to the differences in the indexes of refraction. The angle of divergence is a function of the prism's wedge angle and the wavelength. In commercial Wollaston prisms, this angle can vary from 1 degree to 45 degrees.

#### 3.3. Option 3: One Magneto-Optical Filter in Double Pass

The MOF is a significant contributor to the mass and volume of the magnetograph. For both cells, a collimated beam with incoming linear polarisation is required, ideally with a pupil image inside the cells. To meet this, for both cells, some optical components are required between them. Two cells are also needed, with the magnetic field of the second cell, the Wing Selector (WS), higher than the magnetic field of the first cell because its Zeeman component must be superimposed to the transmission peaks of the Macaluso–Corbino

effect. The alternative here proposed is to have only one MOF with the magnetic field required for the WS and use it in double pass, as shown in Figure 3.

This would reduce volume and mass since only one cell would be needed and the optical components to generate a pupil image in a collimated beam with linear polarisation would not need to be duplicated, with the space reduction associated with the separation between these components. The size required for the cell in this layout is 64 mm side by 30 mm thickness. The dimensions for the layout with the two detectors is 397 mm × 125.5 mm. The points to be evaluated in this option are the effect of having illumination in both directions for a defined direction of the magnetic field. In one pass, the beam would be in favour of this direction, and in the double pass in opposite direction. Would it be possible to set the system so that the second pass is the one in the direction of the magnetic field for the Macaluso–Corbino effect since it is required to have a higher magnetic field for the WS? Two flat mirrors orthogonal to each other and thus not modifying the polarisation state would be used to revert the beam path back to the MOF for a second pass.

The gap between the mirrors separates the input and output axes, which are parallel. The MOF shall be large enough to accept this separation between the input and output beams without vignetting. This idea could be combined with the previous ones using a reimaging system to reduce the beam size, for example, to a half, and thus be able to have the beams associated with the two directions inside the original cell size.

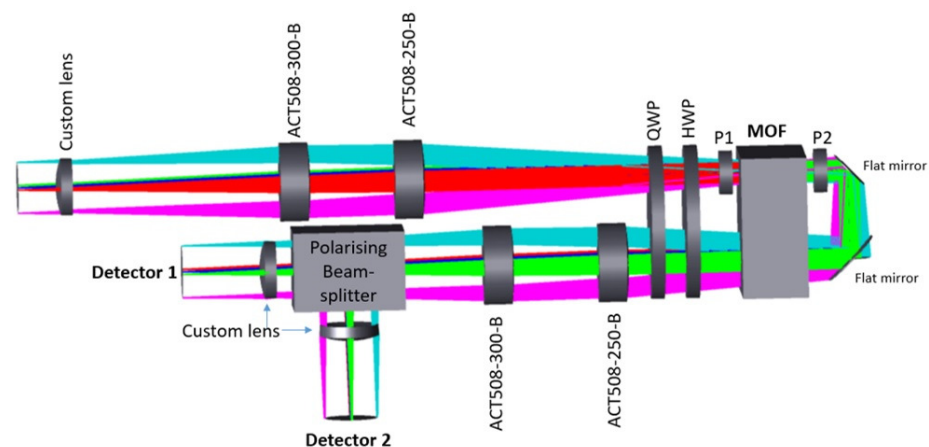


**Figure 3.** Compact magnetograph layout with one cell used in double pass and two detectors to measure the two polarisation components. The colours represent different fields.

### 3.4. Option 4: Application of Slicers for Magnetographs

Image slicers are typically used to slice a field of view. This application is discarded for magnetographs since an image of the full disk is required. However, slicers can be used at different locations and with different functionalities, for example a pupil slicer or a slicer at the image focal plane to arrange the image distribution. A pupil slicer (see Figure 4) would produce two beams with the same field of view. By adding a pupil slicer, each arm would correspond to a polarisation state (Figure 5), in which this separation would be performed before the detector, thus controlling the output direction towards the detector and adding flexibility in the layout. If this were combined with the previous ideas, using a re-imaging system after the telescope focus, the beam size would already be reduced. Thereby, a pupil slicer would produce two beams that could fit within the MOFs (with their original size) and also within one detector. A lateral beam displacement beam splitter could be used as a pupil slicer producing the two parallel beams.

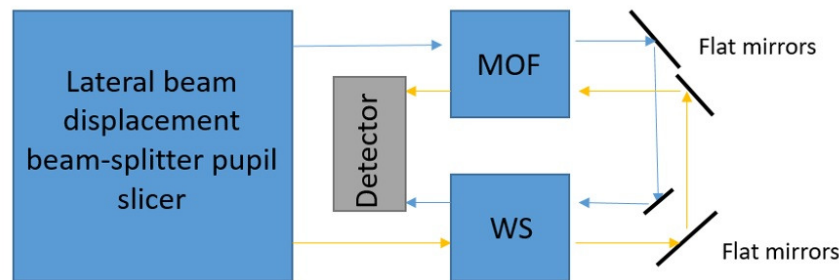


**Figure 4.** Sketch for a compact magnetograph using a pupil slicer generating two output parallel beams, two cells, and only one detector.

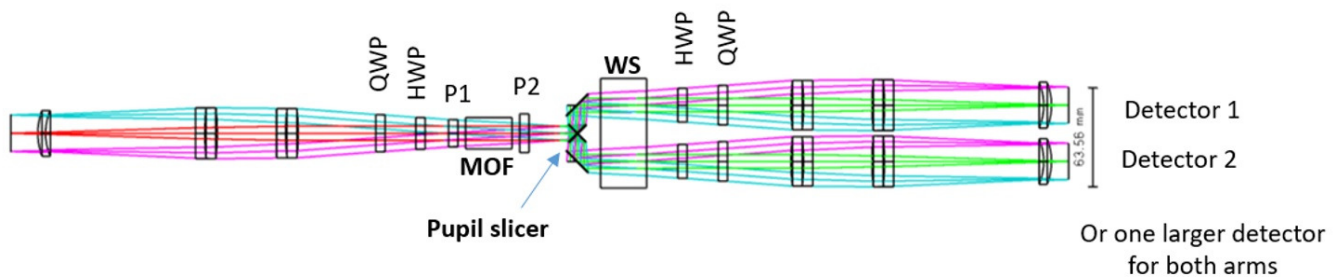


**Figure 5.** Magnetograph layout using a pupil slicer. The colours represent different fields.

## 4. Design of a Miniaturised Solar Magnetograph

### 4.1. Specifications

The specifications, shown in Table 1, are drawn from the HMI instrument's vector telescope on board the Solar Dynamics Observatory and correspond to a solar magnetograph for operational space weather forecasting and space science investigations. The mass of existing solar space magnetographs ranges between 73 and 35 kg. The goal of this research was to reduce the mass to the minimum possible, with a target of 20 kg for the optics. The goal dimensions for the magnetograph are 800 mm × 200 mm × 200 mm.

**Table 1.** Specifications for a miniaturised solar magnetograph for space applications.

| Specifications                       |                              |
|--------------------------------------|------------------------------|
| Field of view                        | 1920 arcsec diameter at 1 AU |
| Telescope diameter                   | 140 mm                       |
| Telescope effective focal length     | 2468 mm                      |
| Telescope F/D                        | F/17.65                      |
| Plate scale at the telescope focus   | 83.58 arcsec/mm              |
| Wavelength                           | 589 nm (Na D line)           |
| Goal dimensions for the magnetograph | 800 mm × 200 mm × 200 mm     |

### 4.2. Optical Design Options

In order to evaluate the optical performance of the magnetograph, without any additional aberration that would be introduced by the telescope, a paraxial lens has been used to generate a beam and telescope focal plane based on the specifications of Table 1. The first optical design (Figure 6) was a 1:1 telecentric system, using 100 mm focal length lenses for collimator and cameras, which allows enough space for the waveplates (QWP and HWP) and polarisers (P1, P2). An intermediate pupil image was reimaged in the middle of each MOF cell (MOF and WS). This enlarges the instrument size, since another pupil image is required for the second cell (WS). A layout based on this idea generates two intermediate pupil images and an intermediate focus. The space from the first camera lens to the second collimator lens is unused. The length of this first design was 832 mm, slightly larger than the specification. Alternative solutions were investigated to reduce the

total length using real lenses, such as the layout of Figure 7, whose length is reduced to 634 mm × 61.5 mm height and provides a pupil image inside each cell. In order to measure the two polarisation components simultaneously, a polarising beam splitter and a second detector were added, as shown in Figure 8, with an increase in the length of the instrument, which is now 650 mm. Most of the optical components for this design are commercial in order to demonstrate feasibility. For space applications, it will be necessary to select space-qualified optical materials.

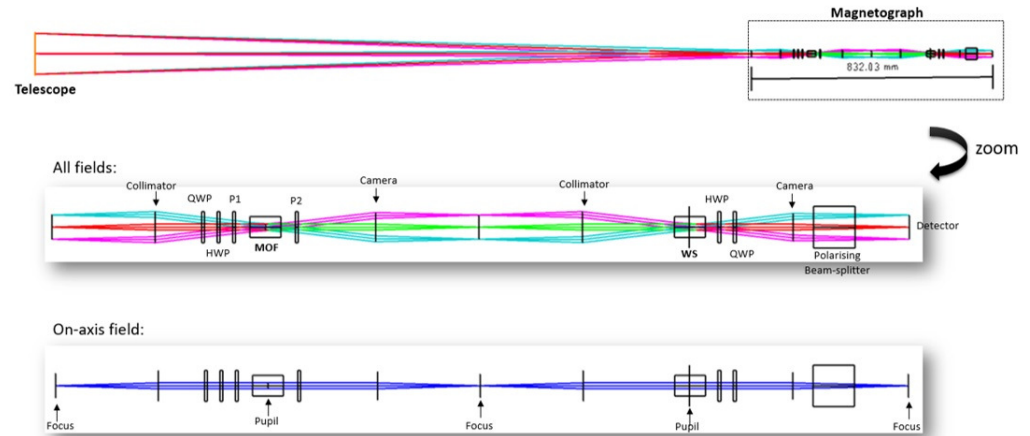


**Figure 6.** Design of a paraxial 1:1 telecentric magnetograph providing a pupil image for each cell and an intermediate focus. The layout on the top includes a paraxial telescope to produce a beam with the specifications defined in Table 1. The layout in the middle includes all fields, and that at the bottom only the on-axis field. The colours represent different fields.

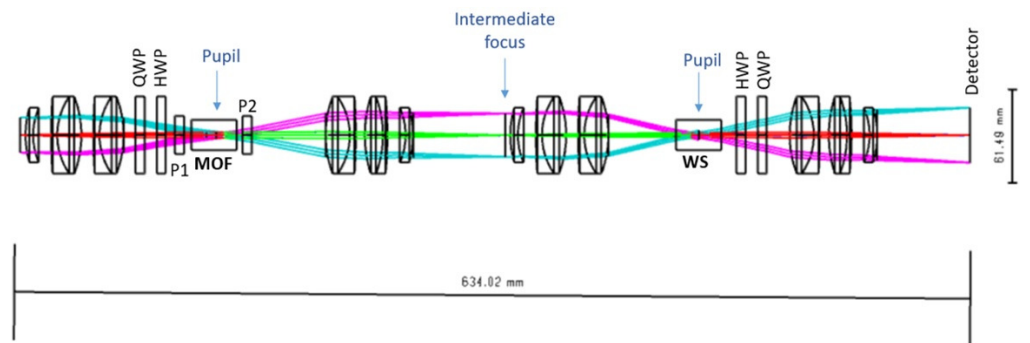


**Figure 7.** Magnetograph design with a pupil image inside each cell and an intermediate focus available. The total length is 634 mm. The colours represent different fields.

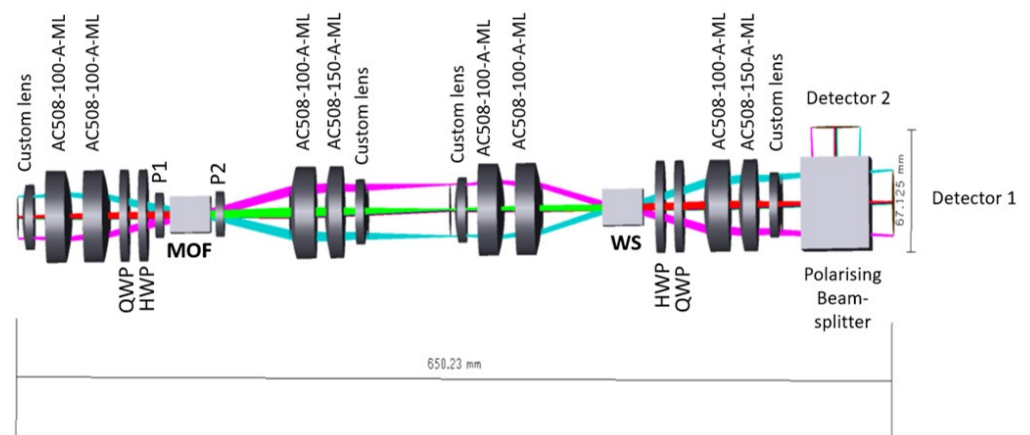


**Figure 8.** Design of a compact magnetograph using mainly commercial components. The colours represent different fields.

Producing only one intermediate pupil, where one of the cells could be centred at and having the second cell nearby or, alternatively, placing both cells close to that pupil, the number of lenses required will be reduced, optimising the efficiency. An example is illustrated in Figure 9 using only one detector to show the concept and in Figure 10 with two detectors to measure the two orthogonal linearly polarised states of the light simultaneously.

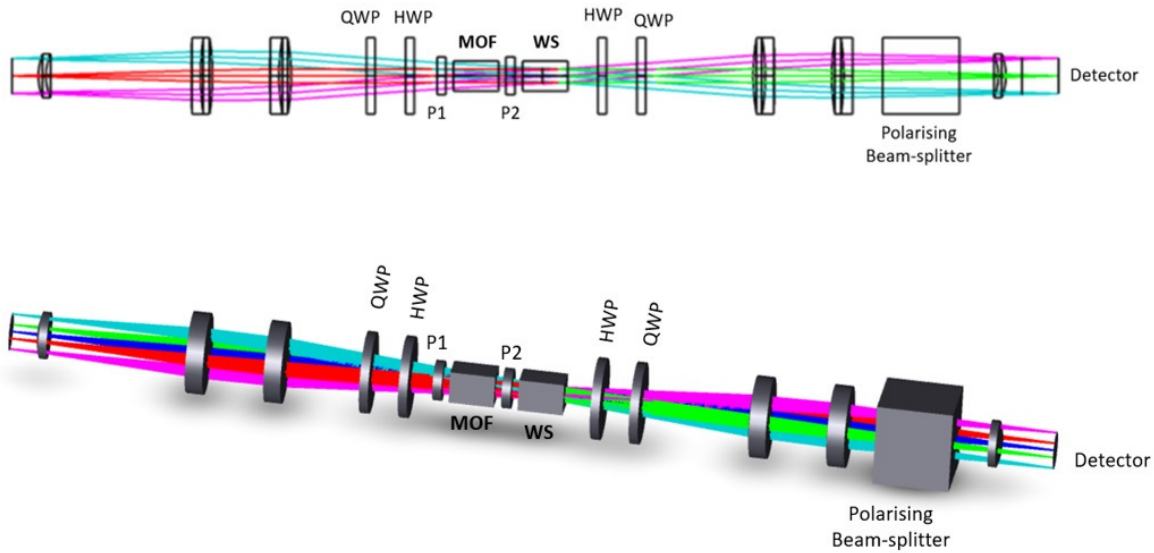


**Figure 9.** Optical design of a magnetograph with one intermediate pupil located within the wing selector (WS) cell, near the MOF. The colours represent different fields.

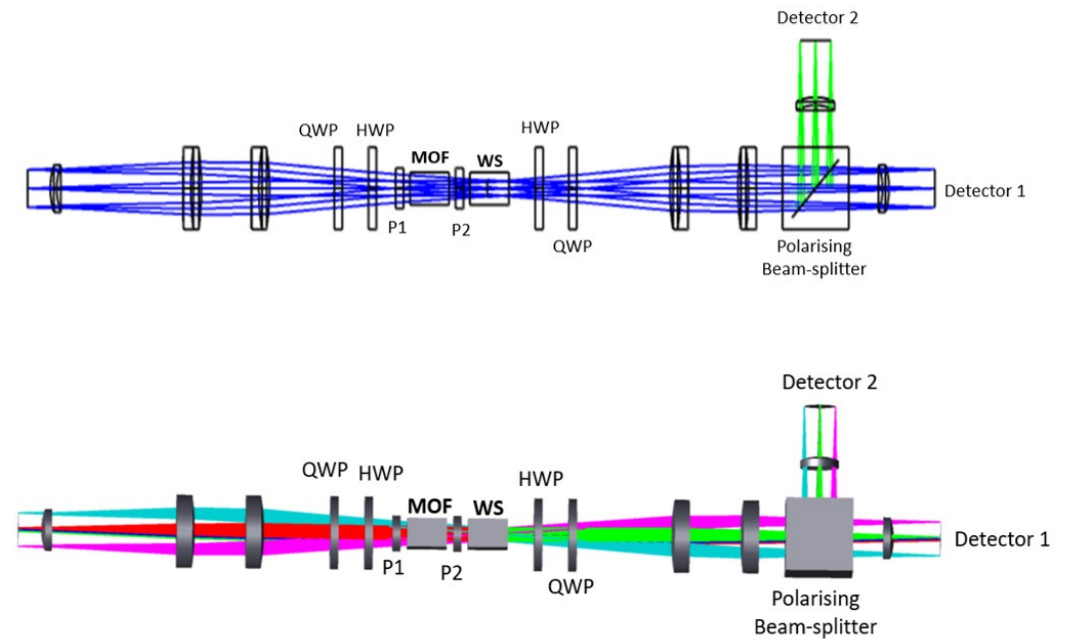


**Figure 10.** Optical design of a magnetograph with one intermediate pupil located within the wing selector (WS) cell, near the MOF, and using two detectors to measure the two orthogonal linearly polarised states of the light simultaneously. The colours represent different fields.

#### 4.3. Final Design and Optical Quality

The studied layout alternatives investigated the feasibility of proposing a magnetograph within the specified envelope (800 mm × 200 mm × 200 mm). Further optimisations led to the final design proposed, reducing the length of the instrument and improving its optical performance.

Our first proposal, shown in Figure 11, is an ultra-compact layout within  $378 \text{ mm} \times 70 \text{ mm} \times 70 \text{ mm}$ . These dimensions are defined for the optics, without including detector sizes and mechanical mounts.

This design has an entrance focal ratio of  $F/17.65$ , with a plate scale of  $83.58 \text{ arcsec/mm}$  at the telescope image focal plane and an instrument final focal ratio of  $F/18.45$ , thus producing a magnification of 1.04. The field of view is  $1920 \text{ arcsec}$  in diameter, equivalent to  $\pm 0.27$  degrees, thus meeting all specifications of Table 1.

The optical components are specified in Figure 12. A custom lens with radii  $42.33 \text{ mm}$  and  $33.58 \text{ mm}$  is placed at  $8 \text{ mm}$  from the focus. Thirty millimetres away, two achromatic doublets from THORLABS are used. The first one, with a focal length of  $180 \text{ mm}$ , is AC508-180-A-ML and the second one, separated by  $10 \text{ mm}$ , has a focal length of  $100 \text{ mm}$  and is AC508-100-A-ML. The quarter and half-wave plates are from Edmund Optics. Six millimetres from the half-wave plate, a linear polariser, P1, is used. Both linear polarisers, P1 and P2, are from THORLABS. The size of the cells (MOF, WS) represented in this layout is  $20 \text{ mm}$  side by  $30 \text{ mm}$  length. An intermediate pupil image is produced within the first cell (MOF). The two achromatic lenses after the second HWP are from THORLABS, the first one, AC508-100-A-ML, with a focal length of  $100 \text{ mm}$  and an achromatic doublet, AC508-180-A-ML, with a focal length of  $180 \text{ mm}$ . The combination of these lenses enables a compact layout. Before the polarising beam splitter, a custom lens, with radii  $44.41 \text{ mm}$  and  $55.37 \text{ mm}$ , compensates for aberrations. The polarising beam-splitter cube, with  $50.8 \text{ mm}$  side, is from THORLABS. The use of mainly commercial optical components was decided in order to build the proposed miniaturised magnetograph and test its performance in the lab.

The proposed solution is very compact, below the specifications for dimensions, and presents a great optical quality almost at the diffraction limit, which is a challenge when considering wide fields of view, short focal lengths, and commercial optical components. The main characteristics are presented in Table 2. Although the proposed design is compact and lightweight, it is not expected to require high-accuracy tolerances. The input and output beams are slow, enabling a depth of focus within which the optical quality is still acceptable. This relaxes tolerances in positioning and angles of incidence. Alignment is more critical in previously considered layouts that share some components, such as the detector or the cell, in order to avoid beam overlapping. No critical aspects have been identified in the proposed layout, however, a detailed tolerance analysis will be performed in later phases, including sensitivity analysis.

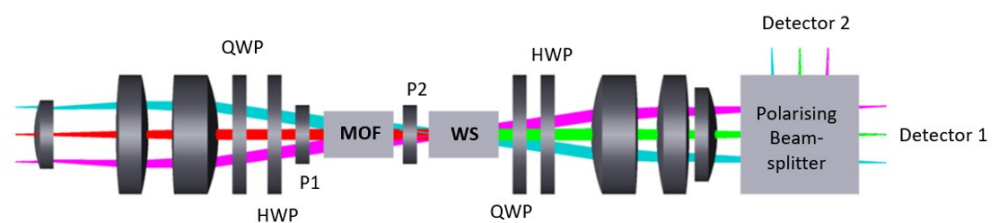


**Figure 11.** Optical design of a miniaturised solar magnetograph with dimensions  $378 \text{ mm} \times 70 \text{ mm}$ . The colours represent different fields.

The size of the image on the detector has a diameter of  $24.17 \text{ mm}$ . If a detector such as that of MDI/SOHO is considered, this would have  $1024 \times 1024$  square pixels of  $21 \mu\text{m}$  side, which leads to a linear size of  $21.50 \text{ mm} \times 21.50 \text{ mm}$ . The image size can be accommodated to the detector size by modifying the last commercial lens, AC508-180-A-ML to AC508-100-A-ML, which has a shorter focal length. This also produces a more compact layout (see Figure 13), with dimensions  $345 \text{ mm} \times 53.9 \text{ mm}$ , and the image size has a diameter of  $18.43 \text{ mm}$  (see Figure 14). Despite being very compact, this layout offers an excellent optical quality, equivalent to that of Figure 15.

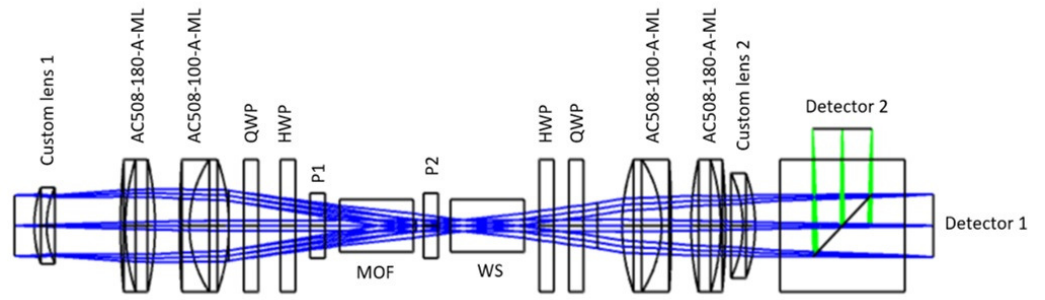


Figure 12. Optical components for the design of a miniaturised solar magnetograph.

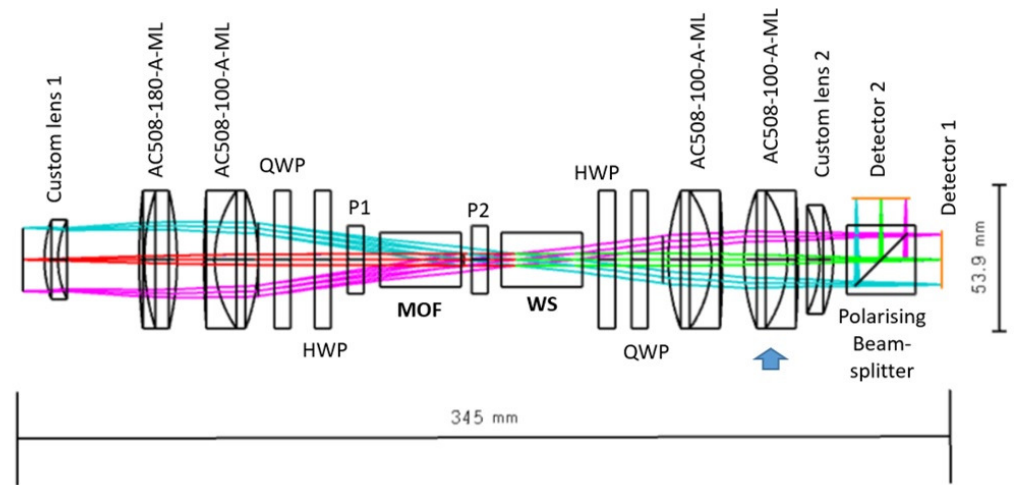


Figure 13. Compact magnetograph design with dimensions 345 mm × 53.9 mm. The colours represent different fields.

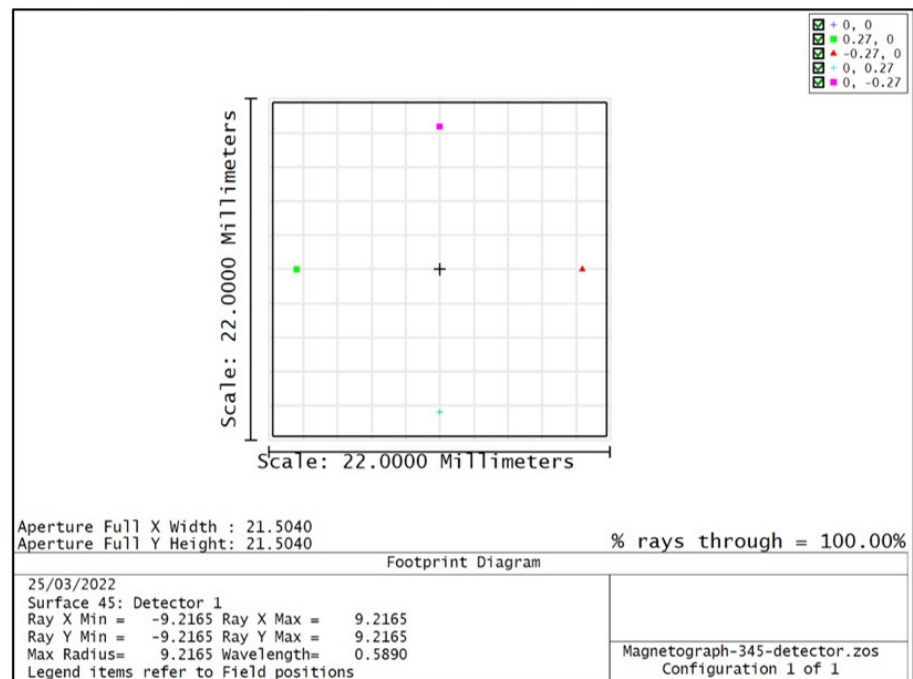
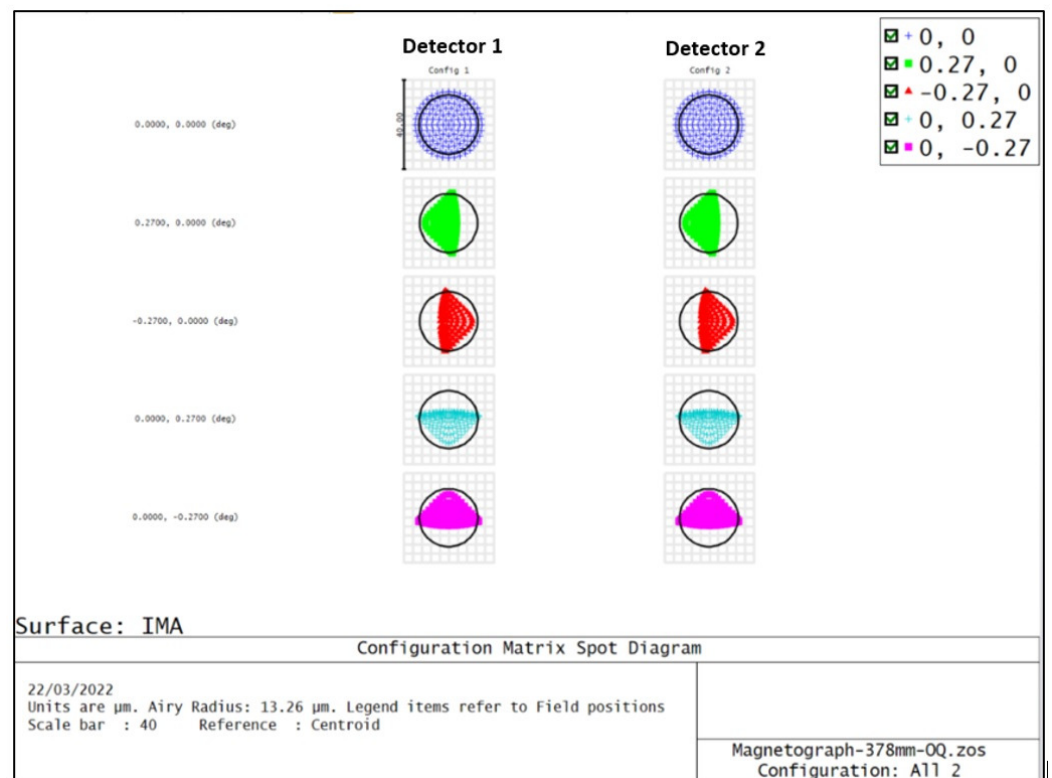


Figure 14. Beam footprint at the detector position showing that with the new design, the image is contained within the detector dimensions.



**Figure 15.** Optical quality obtained at detector 1 (column on the left) and detector 2 (column on the right). For each detector, five field points were defined. The one on the top corresponds to the on-axis field (0,0) and the rest are associated with the values in the legend on the top right, which are defined in degrees. The circle is the Airy disc showing the diffraction limit, within which most of the rays are contained.

A summary of the main investigated optical designs is presented in Table 3, all of them meeting the specifications of Table 1.

**Table 2.** Characteristics of the proposed layout.

| Characteristics of the Proposed Layout |                            |
|--|----------------------------|
| Dimensions                             | 345 mm × 54 mm × 54 mm     |
| Optical quality                        | almost diffraction limited |
| Magnetograph magnification             | 0.79                       |
| Image size                             | 18.43 mm diameter          |
| arcsec/pixel                           | 2.187                      |
| Number of intermediate pupils          | one                        |

**Table 3.** Summary of the main investigated layouts.

| Description  | Length | Layout    |
|--|--------|-----------|
| 1:1 telecentric, two pupils, one per cell            | 634 mm | Figure 8  |
| Only one intermediate pupil, 24.17 mm image diameter | 378 mm | Figure 12 |
| One pupil, 18.43 mm image diameter                   | 345 mm | Figure 13 |

## 5. Conclusions

The main goal of this research was to investigate the feasibility of more compact and lightweight solar magnetographs for space applications. Several novel ideas were evaluated to reduce dimensions. The conclusion of this study is that it is possible to design a miniaturised solar magnetograph with diffraction-limited optical quality contained within

an envelope of 345 mm × 54 mm × 54 mm. The weight of the optics has been significantly reduced with respect to existing solutions. This design has an entrance focal ratio of F/17.65, with a plate scale of 83.58 arcsec/mm at the telescope image focal plane, and it produces a magnification of 0.79. The field of view is 1920 arcsec in diameter, equivalent to ±0.27 degrees. For a low-earth satellite in a near-equatorial orbit, the doppler shift at the sodium D line would be up to 0.015 nm. Given that the MOF filter is not tuneable in wavelength, this would imply a significant orbital change in sensitivity. However, this can be overcome by selecting an orbit at L1 (e.g., SoHO), L2, L4, or L5. Most of the optical components considered for this layout are commercial and, although these are not space qualified, they have been selected in order to prove the concept. This research will continue building the proposed magnetograph and measuring its performance in the lab to complete the feasibility study of miniaturised solar magnetographs and enable this technology for future space missions.

**Author Contributions:** Conceptualization, A.C.R.; Formal analysis, A.C.R. and A.S.; Investigation, A.C.R., L.M.G., A.S. and D.M.L.; Writing—original draft, A.C.R.; Writing—review & editing, L.M.G., A.S. and D.M.L.; Funding acquisition, L.M.G. All authors have read and agreed to the published version of the manuscript.

**Funding:** This research was funded by a Royal Society Enhancement Award. LMG also received funding under the Royal Society University Research Fellowship scheme. DML is grateful to the Science Technology and Facilities Council for the award of an Ernest Rutherford Fellowship (ST/R003246/1).

**Conflicts of Interest:** The authors declare no conflict of interest.

## References

1. Brun, A.S.; Browning, M.K. Magnetism, dynamo action and the solar-stellar connection. *Living Rev. Sol. Phys.* **2017**, *14*, 4. [[CrossRef](#)] [[PubMed](#)]
2. Temmer, M. Space weather: The solar perspective: An update to Schwenn (2006). *Living Rev. Sol. Phys.* **2021**, *18*, 4. [[CrossRef](#)]
3. Forbes, T.G. A review on the genesis of coronal mass ejections. *J. Geophys. Res.* **2000**, *105*, 23153. [[CrossRef](#)]
4. Green, L.M.; Török, T.; Vršnak, B.; Manchester, W.; Veronig, A. The origin, early evolution and predictability of solar eruptions. *Space Sci. Rev.* **2018**, *214*, 46. [[CrossRef](#)]
5. Odstrčil, D.; Pizzo, V.J. Distortion of the interplanetary magnetic field by three-dimensional propagation of coronal mass ejections in a structured solar wind. *J. Geophys. Res.* **1999**, *104*, 28225. [[CrossRef](#)]
6. Pomoell, J.; Poedts, S. EUHFORIA: European heliospheric forecasting information asset. *J. Space Weather Space Clim.* **2018**, *8*, A35. [[CrossRef](#)]
7. de Wijn, A.G.; Casini, R.; Carlile, A.; Lecinski, A.R.; Sewell, S.; Zmarzly, P.; Eigenbrot, A.D.; Beck, C.; Wöger, F.; Knölker, M. The visible spectro-polarimeter of the Daniel K. Inouye Solar Telescope. *Sol. Phys.* **2022**, *297*, 22. [[CrossRef](#)]
8. Scherrer, P.H.; Schou, J.; Bush, R.I.; Kosovichev, A.G.; Bogart, R.S.; Hoeksema, J.T.; Liu, Y.; Duvall, T.L., Jr.; Zhao, J.; Title, A.M.; et al. The Helioseismic and Magnetic Imager (HMI) Investigation for the Solar Dynamics Observatory (SDO). *Sol. Phys.* **2012**, *275*, 207. [[CrossRef](#)]
9. Tsuneta, S.; Ichimoto, K.; Katsukawa, Y.; Nagata, S.; Otsubo, M.; Shimizu, T.; Suematsu, Y.; Nakagiri, M.; Noguchi, M.; Tarbell, T.; et al. The solar optical telescope for the Hinode mission: An overview. *Sol. Phys.* **2008**, *249*, 167. [[CrossRef](#)]
10. Scherrer, P.H.; Hoeksema, J.T.; Bush, R.I. The solar oscillations investigation—Michelson Doppler imager for SOHO. *Adv. Space Res.* **1991**, *11*, 113. [[CrossRef](#)]
11. Solanki, S.K.; del Toro Iniesta, J.C.; Woch, J.; Gandorfer, A.; Hirzberger, J.; Alvarez-Herrero, A.; Appourchaux, T.; Pillet, V.M.; Pérez-Grande, I.; Kilders, E.S.; et al. The polarimetric and helioseismic imager on solar orbiter. *Astron. Astrophys.* **2020**, *642*, A11. [[CrossRef](#)]
12. Agnelli, G.; Cacciani, A.; Fofi, M. The magneto-optical filter: I: Preliminary observations in Na D lines. *Sol. Phys.* **1975**, *44*, 509. [[CrossRef](#)]
13. Forte, R.; Jefferies, S.M.; Berrilli, F.; Moro, D.D.; Fleck, B.; Giovannelli, L.; Murphy, N.; Pietropaolo, E.; Rodgers, W. The MOTH II Doppler-Magnetographs and Data Calibration Pipeline. *Proc. Int. Astron. Union* **2018**, *335*, 335–339. [[CrossRef](#)]
14. Giovannelli, L.; Berrilli, F.; Calchetti, D.; Del Moro, D.; Viavattene, G.; Pietropaolo, E.; Iarlori, M.; Rizi, V.; Jefferies, S.M.; Oliviero, M.; et al. The Tor Vergata Synoptic Solar Telescope (TSST): A robotic, compact facility for solar full disk imaging. *J. Space Weather Space Clim.* **2020**, *10*, 58. [[CrossRef](#)]
15. Calchetti, D.; Viavattene, G.; Terranegra, L.; Pietropaolo, E.; Oliviero, M.; Murphy, N.; Jefferies, S.M.; Giovannelli, L.; Moro, D.D.; Berrilli, F. Tor Vergata Synoptic Solar Telescope: Spectral characterization of potassium KI D1 MOFs. In Proceedings of the Ground-based and Airborne Telescopes VIII, Online, 14–18 December 2020; SPIE: Bellingham, WA, USA, 2020; Volume 11445, p. 114452T.

16. Berrilli, F.; Bigazzi, A.; Roselli, L.; Sabatini, P.; Velli, M.; Alimenti, F.; Cavallini, F.; Greco, V.; Moretti, P.F.; Orsini, S.; et al. The ADAHELI solar mission: Investigating the structure of Sun's lower atmosphere. *Adv. Space Res.* **2010**, *45*, 1191. [[CrossRef](#)]
17. Moretti, P.F.; Berrilli, F.; Bigazzi, A.; Jefferies, S.M.; Murphy, N.; Roselli, L.; Mauro, M.P.D. Future instrumentation for solar physics: A double channel MOF imager on board ASI Space Mission ADAHELI. *Astrophys. Space Sci.* **2010**, *328*, 313. [[CrossRef](#)]
18. Ruzmaikin, A.; Moynihan, P.I.; Vaughan, A.H.; Cacciani, A. Compact Doppler magnetograph. In Proceedings of the Missions to the Sun II, San Diego, CA, USA, 22–23 July 1998; Volume 3442, p. 115. [[CrossRef](#)]

**Disclaimer/Publisher's Note:** The statements, opinions and data contained in all publications are solely those of the individual author(s) and contributor(s) and not of MDPI and/or the editor(s). MDPI and/or the editor(s) disclaim responsibility for any injury to people or property resulting from any ideas, methods, instructions or products referred to in the content.